

# Crystal structures of trimeric HIV envelope with entry inhibitors BMS-378806 and BMS-626529

Marie Pancera<sup>1</sup>, Yen-Ting Lai<sup>1</sup>, Tatsiana Bylund<sup>1</sup>, Aliaksandr Druz<sup>1</sup>, Sandeep Narpala<sup>1</sup>, Sijy O'Dell<sup>1</sup>, Arne Schön<sup>2</sup>, Robert T Bailer<sup>1</sup>, Gwo-Yu Chuang<sup>1</sup>, Hui Geng<sup>1</sup>, Mark K Louder<sup>1</sup> , Reda Rawi<sup>1</sup>, Djade I Soumana<sup>1</sup>, Andrés Finzi<sup>3</sup>, Alon Herschhorn<sup>4</sup>, Navid Madani<sup>4</sup>, Joseph Sodroski<sup>4</sup>, Ernesto Freire<sup>2</sup>, David R Langley<sup>5</sup>, John R Mascola<sup>1</sup>, Adrian B McDermott<sup>1</sup> & Peter D Kwong<sup>1\*</sup>

**The HIV-1 envelope (Env) spike is a conformational machine that transitions between prefusion (closed, CD4- and CCR5-bound) and postfusion states to facilitate HIV-1 entry into cells. Although the prefusion closed conformation is a potential target for inhibition, development of small-molecule leads has been stymied by difficulties in obtaining structural information. Here, we report crystal structures at 3.8-Å resolution of an HIV-1-Env trimer with BMS-378806 and a derivative BMS-626529 for which a prodrug version is currently in Phase III clinical trials. Both lead candidates recognized an induced binding pocket that was mostly excluded from solvent and comprised of Env elements from a conserved helix and the  $\beta$ 20–21 hairpin. In both structures, the  $\beta$ 20–21 region assumed a conformation distinct from prefusion-closed and CD4-bound states. Together with biophysical and antigenicity characterizations, the structures illuminate the allosteric and competitive mechanisms by which these small-molecule leads inhibit CD4-induced structural changes in Env.**

Structure-based drugs have had remarkable impact on the treatment of HIV-1 infection. Since the mid-1990s, when the first structure-based drugs against HIV-1 protease entered clinical use, the prognosis for an HIV-1 infection treated with antiviral therapy has progressed from a less than 50% 10-year survival to an average life expectancy almost indistinguishable from that of the general population<sup>1–3</sup>. In 2015, 16 million people were treated with antiviral therapy against HIV-1, and there are currently over 40 licensed therapeutics that target HIV-1 enzymes (protease, reverse transcriptase and integrase) or the gp41 envelope glycoprotein (Supplementary Results, Supplementary Fig. 1). Currently, however, no FDA-licensed therapeutic directly targets the HIV-1 gp120 envelope glycoprotein.

Three gp120 envelope glycoproteins, along with three gp41 transmembrane subunits, make up the heterodimeric Env trimer, a type 1 fusion machine that facilitates HIV-1 entry through a multistep process involving structural rearrangements of both gp120 and gp41 subunits. First, the prefusion closed conformation of the assembled Env trimer binds a single CD4 (ref. 4), which stabilizes an intermediate state of Env. Binding to additional CD4 molecules induces the formation and exposure of a site on gp120 that is recognized by a co-receptor, either CCR5 or CXCR4. Binding to a co-receptor induces further conformational changes, especially in gp41, which result in the formation of a six-helix bundle and the fusion of the virus and host cell membranes<sup>5,6</sup>.

HIV-1 entry inhibitors have been developed, including the FDA-approved enfuvirtide, which blocks gp41 conformational changes needed for fusion<sup>7,8</sup>, and maraviroc, which binds to the CCR5 co-receptor and prevents the formation of the Env–CCR5 complex<sup>9</sup>. A number of antibodies have also been identified that neutralize over 90% of HIV-1 (refs. 10–13); these primarily recognize the prefusion closed state of Env and block either receptor attachment or

conformational changes required for entry. CD4-mimetic small molecules and miniproteins have been developed that target an interfacial cavity, known as the ‘Phe43’ cavity<sup>14</sup>, which forms in the CD4-bound state of gp120 (refs. 15–18).

An especially promising family of low-molecular-weight HIV-1 entry inhibitors, identified using a viral-infection-based screen<sup>19</sup>, includes BMS-378806 (Bristol-Myers Squibb) and related compounds<sup>19–22</sup>. Clinical assessment of BMS-378806 was abandoned to focus on improved versions<sup>23,24</sup>, and currently, BMS-663068, the prodrug of BMS-626529 (also known as temsavir (GSK2616713); now being developed by ViiV Healthcare), is the top lead inhibitor<sup>25,26</sup>. BMS-663068 has improved *in vitro* and pharmacokinetic properties compared to other family members, including a better potency, a higher barrier for resistance and a good safety profile in humans<sup>27–30</sup>. BMS-663068 is currently being assessed in a Phase III-therapeutic clinical trial. Here we report the structures of small molecules BMS-378806 and BMS-626529 in complex with a soluble mimic of HIV-1-Env trimer, BG505 SOSIP, held in a prefusion conformation by antibodies PGT122 and 35O22 (ref. 31). The structures reveal an induced binding pocket under the  $\beta$ 20–21 loop that is distinct from the Phe43 cavity induced by CD4, suggest an allosteric mechanism of inhibition and provide chemical-level details for inhibitor optimization.

## RESULTS

### Neutralization and binding of BMS-378806 and BMS-626529

We performed neutralization assays to assess the potency of BMS-378806 and BMS-626529 against two BG505 pseudoviruses. BMS-378806 and BMS-626529 neutralized BG505 pseudoviruses *in vitro* with half-maximal inhibitory concentrations ( $IC_{50}$ s) of 1,190 and 14 nM, respectively, for BG505, and 790 and 14 nM, respectively, for BG505 T332N. We also assessed the neutralization of

<sup>1</sup>Vaccine Research Center, National Institute of Allergy and Infectious Diseases, National Institutes of Health, Bethesda, Maryland, USA. <sup>2</sup>Department of Biology, Johns Hopkins University, Baltimore, Maryland, USA. <sup>3</sup>Department of Microbiology, Infectiology and Immunology, Université de Montréal, Montreal, Quebec, Canada. <sup>4</sup>Department of Cancer Immunology and Virology, Dana-Farber Cancer Institute, Boston, Massachusetts, USA.

<sup>5</sup>Computer Assisted Drug Design, Bristol-Myers Squibb, Research and Development, Wallingford, Connecticut, USA. \*e-mail: [pdkwong@nih.gov](mailto:pdkwong@nih.gov)

BMS-378806 and BMS-626529 against a panel of pseudoviruses and observed  $IC_{50}$  values in the range of <1 to 20,000 nM (0.0001–9.5  $\mu\text{g/ml}$ ), indicating highly variable sensitivities of diverse HIV-1 strains to these small molecules (Supplementary Tables 1 and 2). We note that, in this panel, BMS-378806 and BMS-626529 neutralized the BG505 pseudovirus *in vitro* with  $IC_{50}$ s of 170 and 9 nM, respectively (Supplementary Table 1), thus indicating some variation in the assay. The data also confirmed that BMS-626529 is more potent and broad than BMS-378806, with 91% of the viruses neutralized by BMS-626529 compared to 78% by BMS-378806 for an  $IC_{50}$  < 10  $\mu\text{g/ml}$ , and 80% of the viruses neutralized with BMS-626529 compared to 61% with BMS-378806 for an  $IC_{50}$  < 1  $\mu\text{M}$  (Supplementary Tables 1 and 2). We note that BMS-626529 neutralized 59% viruses with an  $IC_{50}$  < 0.01  $\mu\text{g/ml}$  (corresponding to less than 21.1 nM for BMS-626529 and less than 66.7 pmol for the IgG), although coverage by broadly neutralizing antibodies is generally lower at this concentration (Supplementary Table 2).

We used isothermal titration calorimetry (ITC) to determine the affinities of both compounds for a soluble version of the prefusion Env trimer (BG505 SOSIP)<sup>32</sup>, as well as for a stabilized version (DS-SOSIP)<sup>4</sup>, which binds CD4 with an asymmetric single CD4 per Env trimer and is not triggered by soluble CD4 (sCD4). BMS-378806 bound to the BG505 SOSIP trimer with ~14-fold higher affinity than to monomeric gp120 of the same HIV-1 strain (180 compared to 2,600 nM, respectively) and with slightly weaker affinity to DS-SOSIP (210 nM) (Supplementary Fig. 2a). Compared to BMS-378806, BMS-626529 bound with ~2.5-fold higher affinity to BG505 SOSIP and DS-SOSIP with  $K_d$ s of 73 and 87 nM, respectively (Supplementary Fig. 2b). The enthalpy and entropy changes associated with these binding activities were low, similar to what has been described previously<sup>33</sup>, indicating that, unlike CD4, little conformational change occurs in the Env glycoprotein when these compounds bind (Supplementary Fig. 2a,b). Finally, analysis of binding stoichiometry indicated that one BMS-378806 molecule binds to each protomer of the Env trimer (three BMS small molecules per Env trimer). These experiments showed that BMS-378806 and BMS-626529 bind the HIV-1 Env trimer much tighter than monomeric gp120, and similarly recognize SOSIP and DS-SOSIP versions of the trimer (Supplementary Fig. 2).

### Structures of BMS-378806 and BMS-626529 with HIV-1 Env

We individually soaked small-molecule inhibitors into crystals of the HIV-1 Env trimer. The crystals comprised trimeric BG505 SOSIP bound by antibodies PGT122, a 332-glycan dependent antibody<sup>34</sup>, and 35O22, a gp120-gp41 interface antibody<sup>35</sup>, as described previously<sup>31</sup>. The crystals diffracted to a nominal 3.8-Å resolution with both BMS-378806 and BMS-626529. Diffraction was anisotropic, and we used a diffraction anisotropy server (<http://services.mbi.ucla.edu/anisotscale/>) to determine resolution cutoff in each direction<sup>36</sup>. Three sigma ( $3\sigma$ ) data extended to 3 Å along the *c* axis and to less than 4 Å along *a* and *b* axes (see Online Methods regarding details on resolution). Molecular replacement with the drug-free version of the trimer (trimer-PGT122–35O22 with no drug; PDB ID 4TVP<sup>31</sup>) was used to determine phases for the structure, and refinement led to  $R_{\text{work}}/R_{\text{free}}$  values of 0.2453/0.2888 and 0.2723/0.3254 for crystals of with BMS-378806 and BMS-626529, respectively (Supplementary Table 3).

These crystal structures revealed that BMS molecules bind a surface-accessible pocket at the interface between the inner and outer domains of gp120 under the  $\beta$ 20–21 loop, and interact with the C terminus of the  $\alpha$ 1-helix (Fig. 1a; Supplementary Fig. 3a). This pocket is on the other side of  $\beta$ 20–21 relative to the Phe43 cavity where CD4 binds and is only minimally surface accessible (Fig. 1b,c; Supplementary Fig. 3b). Because of the moderate resolution, it was difficult to position unambiguously all atoms of the small molecule, particularly those in the oxoacetamide and piperazine moieties. However, the addition of the methyltriazole ring

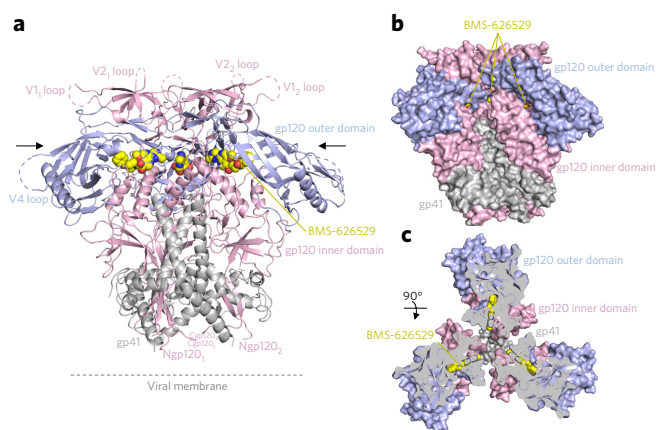


**Figure 1 | HIV-1-Env recognition by small-molecule entry inhibitor BMS-626529.**

(a) Structure of BG505 SOSIP in complex with BMS-626529. Antibodies PGT122 and 35O22, present in the crystallized complex, have been removed for clarity. HIV-1 Env protomers are shown in ribbon representation with gp120 inner domain in pink, gp120 outer domain in blue, and gp41 in gray. BMS-626529 is shown in sphere representation, with atoms colored according to their chemistry: carbon, yellow; nitrogen, blue; and oxygen, red. Subscript numbers relate to corresponding protomers. Black arrows indicate a clip that has been done to visualize the location of BMS-626529 binding in a perpendicular orientation (shown in c). (b) Protomers shown in surface representation and colored as in a with the location of BMS-626529 binding indicated in yellow. (c) 90° rotation from a and b with protomers shown in surface representation.

in BMS-626529, compared to its absence in BMS-378806, allowed an unequivocal determination of overall drug orientation, with the benzoyl ring inserting deep in the conserved drug-induced pocket and the methoxyazaindole ring and triazole ring (for BMS-626529) positioned toward the outside of the cavity (Figs. 2 and 3).

### Details of inhibitor interaction with HIV-1 gp120

Structures of BMS-378806 and BMS-626529 in complex with HIV-1 Env were virtually superimposable, with the methyltriazole ring of BMS-626529 extending toward the trimer axis. Both compounds bound gp120 in a similar manner (Figs. 2b,c and 3c), with BMS-626529 having additional interactions through its methyltriazole ring with Thr202 and Gln432 of gp120 (Fig. 2b). The side chain of Gln432 appeared to rearrange compared to its orientation in the BMS-378806-bound conformation (Fig. 3c) to enable a better fit of the methyltriazole ring. The buried surface area between BMS-378806 and gp120 totaled 870 Å<sup>2</sup>, and that between BMS-626529 and gp120 totaled 1,020 Å<sup>2</sup>. BMS-378806 buried a total of 570 Å<sup>2</sup>, whereas BMS-626529 buried a total of 630 Å<sup>2</sup>. Almost all of the accessible surface areas of the compounds were buried: 99% for BMS-378806 and 94% for BMS-626529 (Supplementary Tables 4 and 5).

The BMS compounds interacted with gp120 mainly through hydrophobic interactions with Trp112, Asp113, Leu116, Val255, Phe382, Ile424, Met426, Trp427, Gln432, Met434 and Met475, and with Thr202 for BMS-626529 only, with each of these residues contributing more than ~10 Å<sup>2</sup> of buried surface area (Figs. 2b and 3c; Table 1; Supplementary Table 4). In addition to purely hydrophobic interactions, aromatic-stacking and hydrogen bonding interactions also contributed to Env-drug interactions. For example, the benzoyl group of the BMS compounds made a parallel and offset  $\pi$ -stacking interaction with Phe382 and Trp427 of gp120, respectively. Other interactions included a hydrogen bond between the backbone NH of Trp427 and one of the oxoacetamide carbonyls of

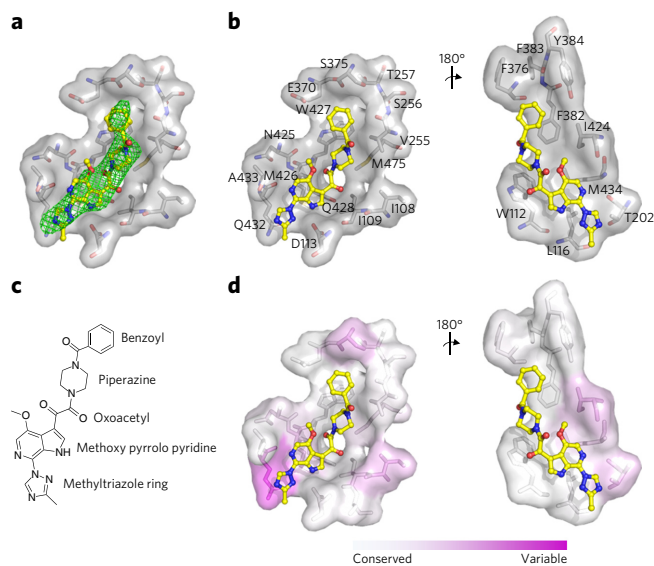


**Figure 2 | Detailed interactions of BMS-626529 with HIV-1 Env gp120.**

(a)  $F_o - F_c$  electron density at  $3\sigma$  of a simulated annealing omit map around BMS-626529 (yellow) shown as green mesh. (b) View from the viral membrane (bottom) of BMS-626529 (left) and view from the trimer apex (top) after  $180^\circ$  rotation (right). Residues that are within 5 Å of BMS-626529 (yellow) are labeled and shown as both stick and surface representation. (c) Chemical formula for BMS-626529. (d) Sequence variability of the binding pocket shown in the same orientations as b.

the compound, and the side chain of Asp113 accepted a hydrogen bond from the azaindole NH group of the compound (Figs. 2b,c; Supplementary Tables 4 and 5).

### Inhibitor-induced conformational changes in Env

The overall conformations of the HIV-1 Env trimers with bound BMS compounds were virtually identical and highly similar to the prefusion closed drug-free structure bound to antibodies PGT122 and 35O22 (PDB ID 4TVP<sup>31</sup>) (Fig. 4a). The C $\alpha$ -r.m.s. deviation between BMS-378806-bound and BMS-626529-bound structures was 0.4 Å over all gp120 residues. C $\alpha$ -r.m.s. deviation between the drug-free 4TVP and BMS-378806-bound structure was 0.6 Å, and that between the drug-free 4TVP and BMS-626529-bound structure was 0.7 Å over all gp120 residues. One region involving the  $\beta$ 20–21 loop, however, differed more substantially between the drug-free 4TVP and the compound-bound structures, displaying a C $\alpha$ -r.m.s. deviation of 1.5–1.8 Å over 13 residues that comprise the loop (residues 423–435) and a C $\alpha$ -r.m.s. deviation of 1.6–2.1 Å over the 8 residues that comprise the majority of the interactions (425–432). Met26 in this loop showed the largest C $\alpha$ -distance difference (2.9–3.0 Å) between compound-bound and ligand-free structures.

The side chains of residues Trp112 (in the  $\alpha$ 1 helix), Asn425, Met426, Trp427, Gln428, Arg429 (all in  $\beta$ 20–21 loop) and Met 475 rearranged to provide a binding pocket and to interact with the BMS compounds (Fig. 4b–e; Supplementary Fig. 4). Thus, a number of local changes in the binding pocket contributed to an induced fit of gp120 for the BMS compounds.

### Structural basis for inhibitor resistance

We analyzed the BMS-compound-bound and drug-free structures to provide atomic-level explanations for phenotypes observed with resistance mutations. When altered, most of the gp120 residues interacting with the BMS molecules affect drug sensitivity<sup>30,37</sup> (Table 1; Supplementary Tables 6 and 7) or confer drug resistance<sup>38</sup>

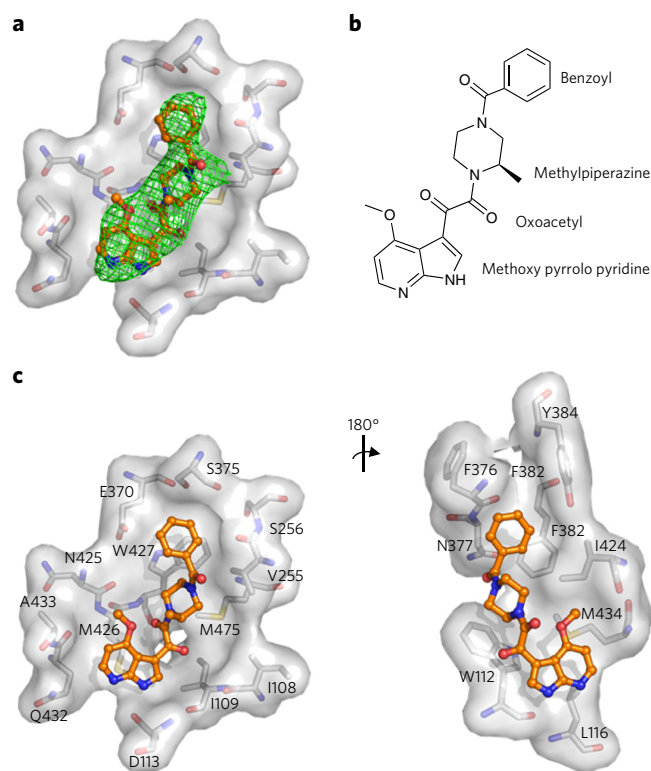


**Figure 3 | Detailed interactions of BMS-378806 with HIV-1 Env gp120.**

(a)  $F_o - F_c$  electron density at  $3\sigma$  of simulated annealing omit map around BMS-378806 (orange) shown as green mesh. (b) Chemical formula for BMS-378806. (c) View from bottom of BMS-378806 and view from the top after  $180^\circ$  rotation. Residues within 5 Å of BMS-378806 (orange) are labeled and shown in both stick and surface representation.

(Table 1). Clinically derived resistance substitutions known to reduce BMS-626529 susceptibility include M426L or S375M, with M434I and M475I contributing to a lesser extent<sup>30</sup>. M426L was also shown to affect BMS-378806 sensitivity, whereas M475S had minor effects<sup>37</sup>. BMS-378806 and BMS-626529 buried  $\sim 30 \text{ \AA}^2$  with Met426, which is part of the  $\beta$ 20–21 loop, and packs directly against the face of the compound azaindole ring. The branched side chain of the M426L substitution is predicted to sterically reduce the size of the compound binding site and to affect the dynamic range of the  $\beta$ 20–21 loop. Interactions between the compound and Met475 buried  $\sim 20 \text{ \AA}^2$  of surface area, and the branched side chain of M475I would be expected to reduce the size of the compound-binding site.

Mutagenesis studies show that S375W substantially affects BMS-378806 sensitivity, whereas a S375A substitution results in a more muted impact<sup>37</sup>. Although direct interactions between the compounds and Ser375 were minimal, in the crystal structure, the  $\beta$ -carbon of Ser375 was positioned near position 4 of the compound's benzoyl ring (buried surface area of  $\sim 7\text{--}10 \text{ \AA}^2$ ). Whereas a S375A mutation would not substantially affect this interaction, larger side chain substitutions, such as a Trp indole or a His imidazole, would likely prevent the entering or the binding of the BMS compounds. Thus, these structures explained why the drugs do not inhibit entry of HIV-2 or SIV, both of which have a Trp residue at position 375, as well as subtype CRF01\_AE, which has a His residue at that position<sup>39</sup>.

In the BMS-compound-bound structures, Met434 packed against Trp112, Leu116, Ala204, Phe210, Phe382, Ile424 and the compound azaindole ring. The branched side chain associated with the M434I change would require either rearrangement of the gp120 inner- and

**Table 1 | Structural basis for resistance mutations**

BG505 Env sequence (HXBc2 numbering)	Mutation	Fold inhibition of BMS-378806 (Madani <i>et al.</i> <sup>37</sup> or from this study; Supplementary Tables 6 and 7)	Clinically derived resistance substitution that reduces susceptibility of BMS-626529 (ref. 30)	Buried surface area (rounded; Å <sup>2</sup> ) with BMS-378806 and BMS-626529 (Supplementary Table 4)	Hydrogen bonds distance (Å) with BMS-378806/ BMS-626529 (Supplementary Table 5)	Structural basis explanation
I109	I109A	This study, >20		6/10		No major effect
W112	W112A	>100		50/57		Loss of hydrophobic interactions
D113	D113A	85		9/27	2.6/2.4	Loss of hydrogen bonds
L116	L116A	This study, ~20		19/21		No major effect
T202	T202K	This study, ~8		17 (BMS-626529)		No major effect
V255	V255A	This study, ~13 (YU2)		25/32		No major effect
S375	S375W	>100		7/10		Fill pocket and prevent compound entry
	S375M		Yes			Fill pocket and prevent compound entry
	S375H					Fill pocket and prevent compound entry
	S375A	1.2				No major effect
F376				7/10		No mutational data
N377	N377L	7.3		<5 for both		No major effect
F382	F382L	>100		20/22		Loss of hydrophobic interactions
Y384	Y384E	This study, >100		<5/6		Loss of hydrophobic interactions
I424	I424A	This study, 78		27/21		Loss of hydrophobic interactions
N425	N425A	This study, ~2		<5/5		No major effect
M426	M426L	>100	Yes	32/29		Loss of hydrophobic interactions
W427	W427F	0.5		26/42	3/3 (main chain)	No major effect
	W427V	Loss of binding <sup>20</sup>				Loss of hydrophobic interactions
	W427A	This study, >100				Loss of hydrophobic interactions
	W427R	This study, >100				Loss of hydrophobic interactions
Q432	K432A	2.3		13/36		No major effect
M434	M434I		Yes	14/15	<4 (BMS-626529) (main chain)	Loss of hydrophobic interactions
M475	M475S	This study, 90		23/18		Loss of hydrophobic interactions
	M475I		Yes			Loss of hydrophobic interactions

Mapping of resistance mutations to BMS-378806, BMS-626529 and other related inhibitors. Listed residues are within 5 Å of the inhibitor.

outer-domain interface or alteration in compound orientation for binding. It should be noted that *in vitro*-selected changes A204D and L116Q or L116P also impact susceptibility<sup>30</sup>. Other substantial interactions between the BMS compounds and gp120 occur through large hydrophobic residues such as Trp112 and Trp427 (with a compound-buried surface area of 25–50 Å<sup>2</sup>). Decreasing the size of the side chains of these residues would likely result in a loss of hydrophobic interactions with the BMS compounds, diminishing inhibitor potency.

Changing Thr257 of gp120 to Arg has been shown to decrease BMS-378806 sensitivity dramatically, whereas T257A has little effect<sup>37</sup>. Although we did not observe direct contact between Thr257

and the BMS compounds, Thr257 packs against Trp427, which is part of the β20–21 loop and interacts directly with the compounds. It is thus possible that introducing a large hydrophilic side chain would prevent the compound from entering or binding properly in a similar manner to the S375W change discussed above.

Additionally, we analyzed neutralization data with BMS-378806 and BMS-626529 from a panel of 208 isolates from diverse clades evaluating all amino acids within 10 Å of the small molecule used for their contribution to neutralization resistance (**Supplementary Fig. 5**). Three variant sequences, at positions 375, 432 and 475, occurred at least three times in the isolate panel and scored above 0.8 with BMS-378806, indicating that these residues are present



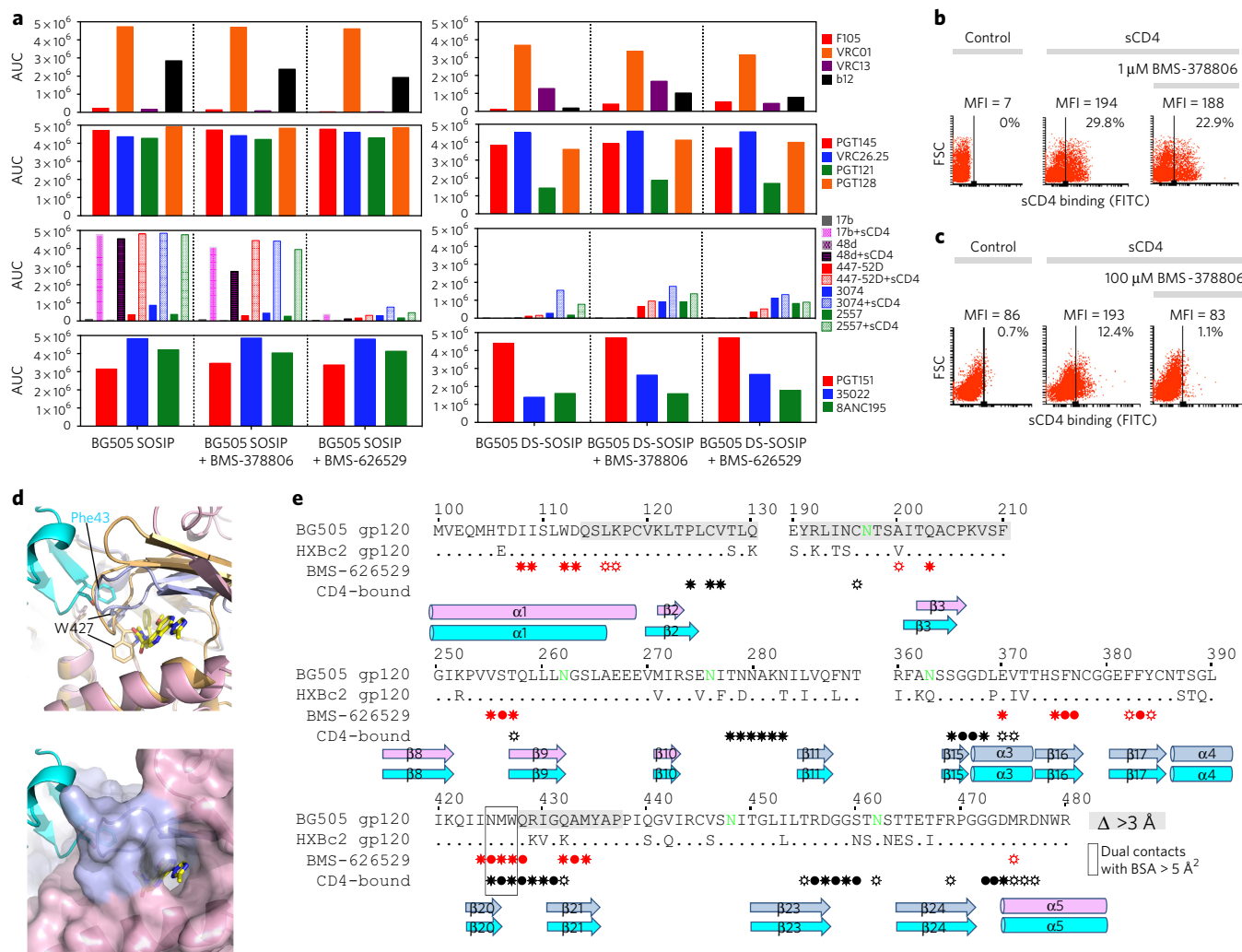


**Figure 5 | Entry inhibition mechanism for BMS-378806 and BMS-626529 small molecules.** (a) MSD-ECLIA of a panel of antibodies binding to BG505 SOSIP and BG505 DS-SOSIP with and without BMS-378806 or BMS-626529. Data quantified by area under the curve (AUC). (b) Flow cytometric analysis of the effect of BMS-378806 on sCD4 binding of the HIV-1 JR-FLΔCT Env expressed on the cell surface. Analysis of sCD4 binding in the presence and absence of BMS-378806. FSC, forward scatter; MFI, mean fluorescence intensity; FITC, fluorescein isothiocyanate. (c) Same as b but at high BMS-378806 concentration. The control shows binding of the FITC-conjugated anti-CD4 antibody to the cells in the absence of sCD4. (d) Top, structures superposition of BMS-626529 (yellow) bound to gp120 (light pink (inner domain) and light blue (outer domain)) in a HIV-1 Env trimeric prefusion closed conformation and CD4-bound conformation (gp120 in light orange and CD4 in cyan). W427 is shown as sticks in both conformations. Bottom, gp120 in a prefusion closed conformation is shown in surface representation. (e) Sequences alignment of BG505 and HXBc2 gp120 regions. Residues in gp120 that make contact with BMS-626529 and CD4 (using the CD4-bound conformation) are indicated with filled circles (for backbone-only interactions), unfilled asterisk (for side chain-only contacts) and filled asterisks (for backbone and side chain contacts) in red (for BMS-626529 contacts) and black (for CD4 contacts), under the sequences. Secondary structure is shown as bars for  $\beta$ -strands; prefusion closed shown in pink and blue as in d, and CD4-bound shown in cyan. gp120 residues that contact both BMS-626529 and CD4, when gp120 is in the postfusion conformation, are boxed in black. Residues that move more than 3 Å between the prefusion and the CD4-bound gp120 conformation are shaded in gray.

while completely blocking the CD4-induced formation and exposure of the gp41 heptad repeat 1 (HR1) coiled coil (Supplementary Fig. 6). Notably, this analysis specifically identified cells that bound sCD4 in the presence of BMS-378806 but did not bind C34-Ig, a gp41 HR2 peptide construct that detects the HR1 coiled coil (Fig. 5b; Supplementary Fig. 6). At high concentrations (100  $\mu$ M), BMS-378806 clearly inhibited the binding of sCD4 (Fig. 5c). These results suggest that the mechanism of HIV-1 inhibition by the BMS compounds may be concentration dependent.

To further clarify the mechanism of inhibition, we compared the structures of the drugs bound to soluble trimer to the CD4-bound structure of gp120 in the monomeric shed or 'postfusion' conformation

that is compatible with co-receptor recognition (PDB ID 3JWD<sup>42</sup>). Although the drugs bound to an Env site distinct from the CD4-binding site, there was overlap in interacting residues; indeed, three residues, Asn425, Met426 and Trp427, contact both BMS compounds and CD4 (each burying more than 5 Å<sup>2</sup> surface area). Thus, the structural data indicate formal competition between binding BMS compounds and CD4 by these residues, which are in the  $\beta$ 20–21 loop, which changes the most in conformation between the drug-free and the CD4-bound structures. Structurally, the critical Trp427 exhibits different conformations in the drug-bound trimer and the CD4-bound monomer and thus cannot accommodate both ligands simultaneously (Fig. 5d,e).

## DISCUSSION

The development of a soluble mimic of the viral spike BG505 SOSIP<sup>32</sup>, which is amenable to crystallization and atomic-level structural analysis, enables a structural understanding of the mechanisms of action for ligands that inhibit HIV-1 entry into cells. In this study, we sought both a mechanistic understanding of entry inhibition by the BMS-378806 family of small-molecule inhibitors and a crystallization template for structure-based design. With Env locked into a prefusion conformation by antibodies PGT122 and 35O22 (refs. 6,31,34,35), we observed that both BMS-378806 and BMS-626529 bound to a conserved pocket under the  $\beta$ 20–21 loop, which CD4 also recognizes<sup>14</sup>. This pocket was previously proposed as a possible binding site for the BMS drugs using mutagenesis data<sup>37</sup> as well as in a recent homology modeling study<sup>43</sup>, unlike docking studies that place these compounds in the Phe43 cavity<sup>44–46</sup>.

There is a general agreement that BMS-378806 and related compounds work only before CD4 binding<sup>21,33</sup>, the nuance here being that CD4 binding can occur with a number of Env conformations, including binding by a single CD4 to a prefusion closed trimer<sup>4,47</sup>, binding within the context of an obligatory ‘high-FRET’ intermediate<sup>6</sup>, and binding in the monomeric gp120 context<sup>14</sup>. Indeed, controversy has existed regarding the mechanism of action of the BMS-378806 family of small-molecule inhibitors<sup>20–22,33,48</sup>. Some studies have shown that the BMS compounds bind gp120 and block its attachment to CD4 (refs. 20,22), while other studies have shown simultaneous binding of the BMS compounds and CD4 to HIV-1 membrane-localized Env trimers and have suggested that inhibition occurs at a later step of the entry process<sup>21,33</sup>. Recently, it has been shown that the BMS compounds stabilize a prefusion closed conformation of Env<sup>6,48</sup> and block Env glycoprotein transitions critical for entry<sup>40</sup>. Site-directed, *in vitro*-selected, and clinical-resistant mutations have helped define the binding region within gp120 for the BMS compounds, and multiple computer modeling studies have been performed to explore possible binding modes and further elucidate the mechanism of action of these small molecules<sup>43,44,49</sup>. However, until now, the experimental structure of a BMS compound bound within the Env trimer has remained elusive.

The BMS compound–Env trimer structures reported here are in agreement with the location of resistance-associated Env changes and explain how the drugs inhibit HIV-1 entry. In concordance with prior published studies<sup>21,22,33</sup>, our data indicate that BMS-378806 and related compounds use multiple mechanisms to inhibit HIV-1 infection. At lower concentrations in which the BMS compounds are first observed to inhibit HIV-1 entry, they stabilize a prefusion conformation of the Env trimer and interfere with Env conformational changes induced by CD4, such as formation and exposure of the gp41 HR1 coiled coil. We note that inhibition by conformational stabilization likely involves alteration of the kinetic transitions the prefusion spike spontaneously undergoes<sup>6</sup>, and such inhibition can have an outsized effect: with BMS-378806 and BMS-626529, we observed a 2.5-fold difference in binding affinity to the BG505 SOSIP trimer and a 19-to-85-fold difference in neutralization of BG505 virus. Consistent with this, BMS-626529 binding to the BG505 SOSIP.664 trimer is accompanied by an unfavorable entropy change, indicating that BMS-626529 binding introduces more order into the Env trimer than BMS-378806 binding. At higher concentrations, where the BMS compounds are observed to inhibit CD4 binding, a mechanism related to that proposed by Langley *et al.*<sup>43</sup> may apply. We observed that the BMS compounds bind under and on the opposite side of the  $\beta$ 20–21 loop from that recognized by CD4, thereby allosterically blocking CD4 attachment. In contrast, the  $\beta$ 20–21 loop in the postfusion conformation (PDB ID 3JWD<sup>42</sup>) is organized and stabilized by CD4 in a way that places Trp427 in the Phe43 binding pocket<sup>50</sup>; this eliminates the BMS compound-binding site and rearranges the parallel  $\beta$ 2-3-21-20 bridging sheet of the prefusion conformation into the

antiparallel  $\beta$ 3-2-21-20 conformation observed in the CD4-bound postfusion state. Overall, our findings clarify both binding mode and mechanism of action. Thus, BMS-626529 and related compounds preferentially recognize a prefusion closed trimer over monomeric gp120 and can only interact with gp120 before CD4 binding. At low concentrations, they stabilize a prefusion conformation of the Env trimer, and at high concentrations, they allosterically interfere with CD4 binding, with three gp120 residues having dual contact with drug and CD4 in their respective high-affinity Env-bound structures.

Received 15 December 2016; accepted 19 July 2017;  
published online 21 August 2017

## METHODS

Methods, including statements of data availability and any associated accession codes and references, are available in the [online version of the paper](#).

## References

- Lima, V.D. *et al.* Continued improvement in survival among HIV-infected individuals with newer forms of highly active antiretroviral therapy. *AIDS* **21**, 685–692 (2007).
- Marcus, J.L. *et al.* Narrowing the gap in life expectancy between HIV-infected and HIV-uninfected individuals with access to care. *J. Acquir. Immune Defic. Syndr.* **73**, 39–46 (2016).
- Vittinghoff, E. *et al.* Combination antiretroviral therapy and recent declines in AIDS incidence and mortality. *J. Infect. Dis.* **179**, 717–720 (1999).
- Kwon, Y.D. *et al.* Crystal structure, conformational fixation and entry-related interactions of mature ligand-free HIV-1 Env. *Nat. Struct. Mol. Biol.* **22**, 522–531 (2015).
- Wyatt, R. & Sodroski, J. The HIV-1 envelope glycoproteins: fusogens, antigens, and immunogens. *Science* **280**, 1884–1888 (1998).
- Munro, J.B. *et al.* Conformational dynamics of single HIV-1 envelope trimers on the surface of native virions. *Science* **346**, 759–763 (2014).
- Wild, C., Greenwell, T. & Matthews, T. A synthetic peptide from HIV-1 gp41 is a potent inhibitor of virus-mediated cell-cell fusion. *AIDS Res. Hum. Retroviruses* **9**, 1051–1053 (1993).
- Oldfield, V., Keating, G.M. & Plosker, G. Enfuvirtide: a review of its use in the management of HIV infection. *Drugs* **65**, 1139–1160 (2005).
- Dorr, P. *et al.* Maraviroc (UK-427,857), a potent, orally bioavailable, and selective small-molecule inhibitor of chemokine receptor CCR5 with broad-spectrum anti-human immunodeficiency virus type 1 activity. *Antimicrob. Agents Chemother.* **49**, 4721–4732 (2005).
- Wu, X. *et al.* Rational design of envelope identifies broadly neutralizing human monoclonal antibodies to HIV-1. *Science* **329**, 856–861 (2010).
- Huang, J. *et al.* Broad and potent neutralization of HIV-1 by a gp41-specific human antibody. *Nature* **491**, 406–412 (2012).
- Muster, T. *et al.* Cross-neutralizing activity against divergent human immunodeficiency virus type 1 isolates induced by the gp41 sequence ELDKWAS. *J. Virol.* **68**, 4031–4034 (1994).
- Huang, J. *et al.* Identification of a CD4-binding-site antibody to HIV that evolved near-pan neutralization breadth. *Immunity* **45**, 1108–1121 (2016).
- Kwong, P.D. *et al.* Structure of an HIV gp120 envelope glycoprotein in complex with the CD4 receptor and a neutralizing human antibody. *Nature* **393**, 648–659 (1998).
- Zhao, Q. *et al.* Identification of *N*-phenyl-*N'*-(2,2,6,6-tetramethyl-piperidin-4-yl)-oxalamides as a new class of HIV-1 entry inhibitors that prevent gp120 binding to CD4. *Virology* **339**, 213–225 (2005).
- LaLonde, J.M. *et al.* Structure-based design, synthesis, and characterization of dual hotspot small-molecule HIV-1 entry inhibitors. *J. Med. Chem.* **55**, 4382–4396 (2012).
- Madani, N. *et al.* Small-molecule CD4 mimics interact with a highly conserved pocket on HIV-1 gp120. *Structure* **16**, 1689–1701 (2008).
- Huang, C.C. *et al.* Scorpion-toxin mimics of CD4 in complex with human immunodeficiency virus gp120 crystal structures, molecular mimicry, and neutralization breadth. *Structure* **13**, 755–768 (2005).
- Wang, T. *et al.* Discovery of 4-benzoyl-1-[(4-methoxy-1*H*-pyrrolo[2,3-*b*]pyridin-3-yl)oxoacetyl]-2- (R)-methylpiperazine (BMS-378806): a novel HIV-1 attachment inhibitor that interferes with CD4-gp120 interactions. *J. Med. Chem.* **46**, 4236–4239 (2003).
- Guo, Q. *et al.* Biochemical and genetic characterizations of a novel human immunodeficiency virus type 1 inhibitor that blocks gp120-CD4 interactions. *J. Virol.* **77**, 10528–10536 (2003).

21. Ho, H.T. *et al.* Envelope conformational changes induced by human immunodeficiency virus type 1 attachment inhibitors prevent CD4 binding and downstream entry events. *J. Virol.* **80**, 4017–4025 (2006).
22. Lin, P.F. *et al.* A small molecule HIV-1 inhibitor that targets the HIV-1 envelope and inhibits CD4 receptor binding. *Proc. Natl. Acad. Sci. USA* **100**, 11013–11018 (2003).
23. Wang, T. *et al.* Inhibitors of human immunodeficiency virus type 1 (HIV-1) attachment. 5. An evolution from indole to azaindoles leading to the discovery of 1-(4-benzoylpiperazin-1-yl)-2-(4,7-dimethoxy-1H-pyrrolo[2,3-c]pyridin-3-yl) ethane-1,2-dione (BMS-488043), a drug candidate that demonstrates antiviral activity in HIV-1-infected subjects. *J. Med. Chem.* **52**, 7778–7787 (2009).
24. Kadow, J., Wang, H.G. & Lin, P.F. Small-molecule HIV-1 gp120 inhibitors to prevent HIV-1 entry: an emerging opportunity for drug development. *Curr. Opin. Investig. Drugs* **7**, 721–726 (2006).
25. Nowicka-Sans, B. *et al.* *In vitro* antiviral characteristics of HIV-1 attachment inhibitor BMS-626529, the active component of the prodrug BMS-663068. *Antimicrob. Agents Chemother.* **56**, 3498–3507 (2012).
26. Brown, J. *et al.* Compartmental absorption modeling and site of absorption studies to determine feasibility of an extended-release formulation of an HIV-1 attachment inhibitor phosphate ester prodrug. *J. Pharm. Sci.* **102**, 1742–1751 (2013).
27. Lalezari, J.P. *et al.* Safety and efficacy of the HIV-1 attachment inhibitor prodrug BMS-663068 in treatment-experienced individuals: 24 week results of A1438011, a phase 2b, randomised controlled trial. *Lancet HIV* **2**, e427–e437 (2015).
28. Nettles, R.E. *et al.* Pharmacodynamics, safety, and pharmacokinetics of BMS-663068, an oral HIV-1 attachment inhibitor in HIV-1-infected subjects. *J. Infect. Dis.* **206**, 1002–1011 (2012).
29. Ray, N. *et al.* Prediction of virological response and assessment of resistance emergence to the HIV-1 attachment inhibitor BMS-626529 during 8-day monotherapy with its prodrug BMS-663068. *J. Acquir. Immune Defic. Syndr.* **64**, 7–15 (2013).
30. Zhou, N. *et al.* Genotypic correlates of susceptibility to HIV-1 attachment inhibitor BMS-626529, the active agent of the prodrug BMS-663068. *J. Antimicrob. Chemother.* **69**, 573–581 (2014).
31. Pancera, M. *et al.* Structure and immune recognition of trimeric pre-fusion HIV-1 Env. *Nature* **514**, 455–461 (2014).
32. Sanders, R.W. *et al.* A next-generation cleaved, soluble HIV-1 Env trimer, BG505 SOSIP.664 gp140, expresses multiple epitopes for broadly neutralizing but not non-neutralizing antibodies. *PLoS Pathog.* **9**, e1003618 (2013).
33. Si, Z. *et al.* Small-molecule inhibitors of HIV-1 entry block receptor-induced conformational changes in the viral envelope glycoproteins. *Proc. Natl. Acad. Sci. USA* **101**, 5036–5041 (2004).
34. Walker, L.M. *et al.* Broad neutralization coverage of HIV by multiple highly potent antibodies. *Nature* **477**, 466–470 (2011).
35. Huang, J. *et al.* Broad and potent HIV-1 neutralization by a human antibody that binds the gp41-gp120 interface. *Nature* **515**, 138–142 (2014).
36. Strong, M. *et al.* Toward the structural genomics of complexes: crystal structure of a PE/PPE protein complex from *Mycobacterium tuberculosis*. *Proc. Natl. Acad. Sci. USA* **103**, 8060–8065 (2006).
37. Madani, N. *et al.* Localized changes in the gp120 envelope glycoprotein confer resistance to human immunodeficiency virus entry inhibitors BMS-806 and #155. *J. Virol.* **78**, 3742–3752 (2004).
38. Zhou, N. *et al.* In vivo patterns of resistance to the HIV attachment inhibitor BMS-488043. *Antimicrob. Agents Chemother.* **55**, 729–737 (2011).
39. Schader, S.M. *et al.* HIV gp120 H375 is unique to HIV-1 subtype CRF01\_AE and confers strong resistance to the entry inhibitor BMS-599793, a candidate microbicide drug. *Antimicrob. Agents Chemother.* **56**, 4257–4267 (2012).
40. Herschhorn, A. *et al.* A broad HIV-1 inhibitor blocks envelope glycoprotein transitions critical for entry. *Nat. Chem. Biol.* **10**, 845–852 (2014).
41. Herschhorn, A. *et al.* Release of gp120 restraints leads to an entry-competent intermediate state of the HIV-1 envelope glycoproteins. *MBio* **7**, e01598–16 (2016).
42. Pancera, M. *et al.* Structure of HIV-1 gp120 with gp41-interactive region reveals layered envelope architecture and basis of conformational mobility. *Proc. Natl. Acad. Sci. USA* **107**, 1166–1171 (2010).
43. Langley, D.R. *et al.* Homology models of the HIV-1 attachment inhibitor BMS-626529 bound to gp120 suggest a unique mechanism of action. *Proteins* **83**, 331–350 (2015).
44. Kong, R., Tan, J.J., Ma, X.H., Chen, W.Z. & Wang, C.X. Prediction of the binding mode between BMS-378806 and HIV-1 gp120 by docking and molecular dynamics simulation. *Biochim. Biophys. Acta* **1764**, 766–772 (2006).
45. Teixeira, C., Serradji, N., Maurel, F. & Barbault, F. Docking and 3D-QSAR studies of BMS-806 analogs as HIV-1 gp120 entry inhibitors. *Eur. J. Med. Chem.* **44**, 3524–3532 (2009).
46. Li, L., Chen, H., Zhao, R.N. & Han, J.G. The investigations on HIV-1 gp120 bound with BMS-488043 by using docking and molecular dynamics simulations. *J. Mol. Model.* **19**, 905–917 (2013).
47. Liu, Q. *et al.* Quaternary contact in the initial interaction of CD4 with the HIV-1 envelope trimer. *Nat. Struct. Mol. Biol.* **24**, 370–378 (2017).
48. Guttman, M. *et al.* CD4-induced activation in a soluble HIV-1 Env trimer. *Structure* **22**, 974–984 (2014).
49. Da, L.T., Quan, J.M. & Wu, Y.D. Understanding the binding mode and function of BMS-488043 against HIV-1 viral entry. *Proteins* **79**, 1810–1819 (2011).
50. Shrivastava, I.H., Wendel, K. & LaLonde, J.M. Spontaneous rearrangement of the  $\beta 20/\beta 21$  strands in simulations of unliganded HIV-1 glycoprotein, gp120. *Biochemistry* **51**, 7783–7793 (2012).

## Acknowledgments

We thank J. Stuckey for assistance with figures, members of Structural Biology and Structural Bioinformatics Core Sections, Vaccine Research Center for discussions and comments on the manuscript. We thank J. Baalwa (University of Alabama at Birmingham), D. Ellenberger (National Cancer Institute, NIH), F. Gao (Duke University), B. Hahn (University of Pennsylvania), K. Hong (Chinese Center for Disease Control and Prevention), J. Kim (The International Vaccine Institute), F. McCutchan (Military HIV Research Program), D. Montefiori (Duke University), L. Morris (National Institute of Communicable Diseases), J. Overbaugh (Fred Hutchinson Cancer Research Center), E. Sanders-Buell (Military HIV Research Program), G. Shaw (University of Pennsylvania), R. Swanstrom (University of North Carolina at Chapel Hill), M. Thomson (Instituto de Salud Carlos III), S. Tovanabutra (Military HIV Research Program), C. Williamson (University of Cape Town) and L. Zhang (China Medical University Shenyang) for contributing the HIV-1 envelope plasmids used in our neutralization panel. We thank D. Burton (The Scripps Research Institute) and M. Feinberg (International AIDS Vaccine Initiative) for antibody PGT122 and M. Connors (National Institute of Allergy and Infectious Diseases, NIH) for antibody 35O22 used in structural analysis. Funding was provided by the Intramural Research Program of the Vaccine Research Center, National Institute of Allergy and Infectious Diseases, the Intramural AIDS Targeted Antiretroviral Program, the National Institute of General Medical Sciences, National Institutes of Health (J.S.), the National Science Foundation MCB-1157506 (E.F.) and the National Institutes of Health GM56550 (E.F.). Use of sector 22 (Southeast Region Collaborative Access team) at the Advanced Photon Source was supported by the US Department of Energy, Basic Energy Sciences, Office of Science, under contract no. W-31-109-Eng-38.

## Author contributions

M.P. determined the structures with assistance from Y.-T.L., G.-Y.C., D.I.S., D.R.L. and P.D.K. T.B. and G.-Y.C. assisted in resistance analysis. S.N. and A.B.M. performed antigenic analyses. S.O'D., R.T.B., M.K.L. and J.R.M. performed neutralization experiments. A.S. and E.F. performed isothermal titration calorimetry experiments. A.D. expressed proteins, and H.G. and D.I.S. purified proteins. R.R. performed sequence entropy analysis. A.F., A.H., N.M. and J.S. contributed mutagenesis analyses and competition analysis with CD4. M.P. and P.D.K. analyzed the data and wrote the paper, with contributions from J.S. and D.R.L.

## Competing financial interests

The authors declare competing financial interests: details accompany the [online version of the paper](#).

## Additional information

Any supplementary information, chemical compound information and source data are available in the [online version of the paper](#). Reprints and permissions information is available online at <http://www.nature.com/reprints/index.html>. Publisher's note: Springer Nature remains neutral with regard to jurisdictional claims in published maps and institutional affiliations. Correspondence and requests for materials should be addressed to P.D.K.

## ONLINE METHODS

**Proteins expression and purification.** Proteins were purified as described previously<sup>31</sup>. Briefly, BG505 SOSIP was cotransfected with furin plasmid into GnTi<sup>-</sup> cells (ATCC (Cat no. CRL-3022)). Supernatant was purified over 2G12 affinity column followed by size-exclusion chromatography in 5 mM HEPES, 150 mM NaCl, and 0.02% azide. BG505 DS-SOSIP was also expressed in GnTi<sup>-</sup> cells, purified over 2G12 affinity column and S200 in the same buffer. PGT122 and 35O22 Fabs were made as described<sup>31</sup>. Heavy and light chains of each IgG were co-transfected in GnTi<sup>-</sup> cells. Supernatants were purified over protein A, antigen-binding fragments (Fabs) were obtained by digesting IgGs modified to have an HRV3C cleavage site in the hinge region with HRV3C enzyme, and the resultant Fabs purified through S200.

**Small-molecule inhibitors.** BMS-378806 and BMS-626529 were purchased from APEX BIO, catalog #B1533 and #A3253, respectively, with a purity of 98.00% and 98.53%, respectively.

**Isothermal titration calorimetry (ITC).** The binding of BMS-378806 and BMS-626529 to HIV-1 Env trimer, BG505 SOSIP and DS-SOSIP, and BG505 gp120 monomer was studied by ITC using a VP-ITC from MicroCal/Malvern Instruments Ltd. (Northampton, MA). The proteins were dialyzed against PBS, pH 7.5, before the experiments. Titrations were performed at 25 °C by injecting aliquots of the inhibitor solution into the calorimetric cell (volume ~1.4 mL) containing either one of the two proteins prepared at ~3 μM in buffer with 2% DMSO. In the case of the Env trimer, the protein concentration corresponds to that of the protomer. BMS-378806 and BMS-626529 were first dissolved in 100% DMSO at concentrations of 10 or 20 mM, which were then diluted into PBS with additional DMSO to their desired concentrations in the presence of 2% DMSO. The concentration of inhibitor in the syringe was 60 and 120 μM for the titrations of the Env trimer and the gp120 monomer, respectively, and the solution was injected in aliquots of 10 μL. Results shown are representative of those obtained in three experiments.

**HIV-1 neutralization assays.** Neutralization was measured using single-round-of-infection HIV-1 Env pseudoviruses and TZM-bl target cells, as described previously<sup>51,52</sup>. Briefly, pseudoviruses were incubated with serial dilutions of antibodies or drug compounds, then added to TZM-bl target cells that have a luciferase reporter gene. After 2 d, infection of target cells was measured by luciferase activity. Assays with drug compounds were performed with 1% DMSO in all wells. Neutralization curves were fit by nonlinear regression using a 5-parameter hill slope equation as previously described<sup>52</sup>. The sensitivity of a panel of HIV-1<sub>HXBc2</sub> and HIV-1<sub>YU2</sub> mutants to inhibition by BMS-378806 was determined as described in the legend to **Supplementary Table 6**.

**Crystallization and data collection.** Crystals of BG505 SOSIP, PGT122 and 35O22 were obtained as described previously<sup>31</sup> in 0.2 M LiSO<sub>4</sub>, 16% isopropanol, 5.32% PEG 1500 and 0.1 M sodium acetate pH 5.5 by the vapor diffusion method. The drugs—BMS-378806 and BMS-626529—were dissolved in mother liquor solution containing 0.2 M LiSO<sub>4</sub>, 20% isopropanol, 6.65% PEG 1500, and 0.1 M sodium acetate pH 5.5 at 1 μM concentration. The stabilizing solution containing the drug was then added to the drops containing the crystals for a period of 5 min to 1 h. Oil was then added to the drop, and crystals suitable for diffraction were analyzed. Diffraction data were collected at APS ID22 and processed using HKL2000 (ref. 53). The nominal overall resolution was determined as the highest resolution for which the completeness was greater than 50% and the ratio of the measured intensity versus the error in intensity was greater than 2.0. Thus, for both BMS-378806 and BMS-626529 with BG505 SOSIP complexes, the nominal overall resolution was 3.8 Å. The BMS-378806 and BMS-626529 with BG505 SOSIP complexes crystal diffraction data were then assessed for anisotropy through use of the Diffraction Anisotropy Server (<http://services.mbi.ucla.edu/anisotropy>)<sup>36</sup>, which indicates the resolution at which  $F/\sigma$  drops below 3.0 along  $a$ ,  $b$ , and  $c$  axes; for the two lattices, these were 3.8 Å, 3.8 Å, and 3.0 Å, respectively. Because we sought to use as much of the data as possible for refinement, we used the overall resolution described above to define the resolution of the  $a$  and  $b$  axes, with

the resolution limit for the  $c$  axis defined by the Diffraction Anisotropy Server. (We note that other investigators have determined overall resolutions using the following equation:  $\text{Res}(\text{eff}) = (\text{high resolution})(\text{completeness})^{(-1/3)}$  (ref. 54), where  $\text{Res}(\text{eff})$  is effective resolution. For the BMS-378806–BG505 SOSIP complex, the untruncated data had a completeness of 81.5%, and the effective resolution is calculated as  $\text{Res}(\text{eff}) = (3.0)(0.815)^{(-1/3)} = 3.2$  Å. For the BMS-626529–BG505 SOSIP complex, the untruncated data had a completeness of 85.6%, and an effective resolution  $\text{Res}(\text{eff}) = (3.0)(0.856)^{(-1/3)} = 3.2$  Å. These alternatively defined resolutions are 0.6 Å higher than our 50% completeness,  $2I/\sigma$ -defined overall resolution. Additionally, the effective resolution using the truncated data for the BMS-378806 complex and the BMS-626529 complex, which had a completeness of 51.7% and 54.06, respectively, are  $\text{Res}(\text{eff}) = (3.0)(0.517)^{(-1/3)} = 3.7$  Å and  $\text{Res}(\text{eff}) = (3.0)(0.546)^{(-1/3)} = 3.7$  Å, respectively. We also report the  $CC_{1/2}$  value of the highest resolution shell (0.450 at 3.0 Å for BMS-378806/BG505 SOSIP complex; 0.141 at 3.0 Å for BMS-626529/BG505 SOSIP complex);  $CC_{1/2}$  values of >0.15 are reported to be significant<sup>55</sup>).

**Structure solution and refinement.** The structure of BMS-378806 and BMS-626529 in complex with BG505 SOSIP/PGT122/35O22 Fab was solved by molecular replacement using Phaser as implemented in CCP4 (ref. 56) using the non-drug-complex structure, PDB ID 4TV<sup>31</sup>, as a search model. Small molecules were manually fitted using COOT<sup>57</sup> and refinement of the structures was with Phenix<sup>58</sup> using optimization of X-ray/stereochemistry and X-ray/ADP weight. CIF files for the small molecules were obtained using ELBOW in Phenix. The refinement statistics are summarized in **Supplementary Table 3**. For the BMS-378806 structure in complex with BG505 SOSIP/PGT122/35O22 Fabs, the overall score from Molprobit<sup>59</sup> was 1.85, with a clash score of 5.59, Ramachadran favored of 92.5% and Ramachadran allowed of 99.3%. For the BMS-626529 structure in complex with BG505 SOSIP/PGT122/35O22 Fabs, the overall score from Molprobit was 1.97, with a clash score of 5.54, Ramachadran favored of 92.1% and Ramachadran allowed of 99.4%. Structural figures were made with Pymol<sup>60</sup>.

**Sequence conservation calculation.** Sequence conservation was calculated based on the HIV-1 filtered web alignment of the year 2015, downloaded from the Los Alamos HIV sequence database (<https://www.hiv.lanl.gov/>). The conservation values for each HXB2 position were obtained applying R, in particular the bio3d package function `conserv` with the input argument “method” set to “identity”.

**Antigenic analysis of BG505 SOSIP and DS-SOSIP in the presence of the drugs BMS-378806 and BMS-626529 by MSD-ECLIA.** Standard 96-well bare MULTI-ARRAY Meso Scale Discovery (MSD) Plates (MSD; cat# L15XA-3) were coated with a panel of HIV neutralizing (VRC01, b12, VRC13, PGT121, PGT128, 2G12, PGT145, CAP256-VRC26.25, 35O22, 8ANC195, PGT151), non-neutralizing monoclonal antibodies (F105, 17b (+sCD4), 48D (+sCD4) and 447-52D (+sCD4), 3074 (+sCD4), 2557 (+sCD4)) and non-cognate antibodies (anti-influenza antibody CR9114, and anti-RSV antibody, D25) at a concentration of 4 μg/mL in duplicates (30 μL/well), after dilution in 1× PBS. and kept overnight at 4 °C. The next day, the plates were washed with 0.05% Tween-20 in 1× PBS and blocked with 150 μL of 5% (w/v) MSD Blocker A (MSD; cat# R93BA-4) for 1 h at room temperature on a vibrational shaker (Heidolph TITRAMAX 100; cat# P/N: 544-11200-00) at 650 r.p.m. BG505 SOSIP and DS-SOSIP were pre-incubated for 1 h with BMS-378806 or BMS-626529 at 1:10 molar ratio of trimer:drug. The trimer or trimer–drug complex were titrated in twofold serial dilutions starting at 5 μg/mL concentration in assay diluent (1% (w/v) MSD blocker A + 0.05% Tween-20). For soluble CD4 (sCD4) induction, trimer–trimer–drug complex were combined with sCD4 at a constant molar concentration of 1 μM before being added to the MSD plate. After the incubation with blocking buffer was complete, the plates were washed and the diluted trimer was transferred (25 μL/well) to the MSD plates and incubated for 2 h on the vibrational shaker at 650 r.p.m. After the 2 h incubation with trimer, plates were washed again and 2G12 antibody labeled with MSD SULFOTAG (MSD; cat #R91AO-1) at a conjugation ratio of 1:15 (2G12:SULFOTAG), which was diluted in assay diluent at 2 μg/mL and added to the plates (25 μL/well), then incubated for 1 h on the vibrational shaker

at 650 r.p.m. Plates were washed and read using the 1× read buffer (MSD Read Buffer T (4×); cat# R92TC-1) on MSD Sector Imager 2400. Results shown are representative of those obtained in three experiments. All antibodies were expressed by transient transfection, after validation of antibody sequence, and reacted with control antigens such as BG505 DS-SOSIP as previously described<sup>4</sup>.

**Flow cytometry.** HIV-1 JR-FLΔCT Env plasmid was transfected with Effectene transfection reagent (Qiagen) into 293T cells following the manufacturer's instructions. 48–72 h later, cells were detached with 5 mM EDTA–PBS. 0.5–1 million cells were incubated briefly with 1 or 100 μM of BMS-378806, in some cases followed by sCD4 (20 μg/ml except in Fig. 5c, where 100 μg/ml sCD4 was used) and then C34-Ig (final concentration 20 μg/mL). After 30 min incubation, the cells were washed twice. Allophycocyanin (APC)-conjugated F(ab)<sub>2</sub> fragment donkey anti-human IgG antibody (1:100 dilution; catalog no. 709-136-149; Jackson ImmunoResearch Laboratories) and fluorescein isothiocyanate-conjugated anti-CD4 antibody (1:33 dilution, E-biosciences) were then added to the cells for 15 min. Cells were washed twice and analyzed with a BD FACSCanto II flow cytometer (BD Biosciences). Results shown are representative of those obtained in two experiments.

**Data availability.** Coordinates and structure factors for the crystal structures of BMS-378806 and BMS-626529 have been deposited in the protein databank (PDB) under accessions numbers 5U7M and 5U7O, respectively, with structure factors both unprocessed and processed through the Diffraction Anisotropy

Server. All other data generated or analyzed during this study are included in this published article (and its supplementary information files) or are available from the corresponding author on reasonable request.

51. Li, M. *et al.* Human immunodeficiency virus type 1 env clones from acute and early subtype B infections for standardized assessments of vaccine-elicited neutralizing antibodies. *J. Virol.* **79**, 10108–10125 (2005).
52. Seaman, M.S. *et al.* Tiered categorization of a diverse panel of HIV-1 Env pseudoviruses for assessment of neutralizing antibodies. *J. Virol.* **84**, 1439–1452 (2010).
53. Otwinowski, Z. & Minor, W. Processing of X-ray diffraction data collected in oscillation mode. *Methods Enzymol.* **276**, 307–326 (1997).
54. Weiss, M.S. Global indicators of X-ray data quality. *J. Appl. Crystallogr.* **34**, 130–135 (2001).
55. Karplus, P.A. & Diederichs, K. Linking crystallographic model and data quality. *Science* **336**, 1030–1033 (2012).
56. Collaborative Computational Project, Number 4. The CCP4 suite: programs for protein crystallography. *Acta Crystallogr. D Biol. Crystallogr.* **50**, 760–763 (1994).
57. Emsley, P. & Cowtan, K. Coot: model-building tools for molecular graphics. *Acta Crystallogr. D Biol. Crystallogr.* **60**, 2126–2132 (2004).
58. Adams, P.D. *et al.* PHENIX: a comprehensive Python-based system for macromolecular structure solution. *Acta Crystallogr. D Biol. Crystallogr.* **66**, 213–221 (2010).
59. Davis, I.W., Murray, L.W., Richardson, J.S. & Richardson, D.C. MOLPROBITY: structure validation and all-atom contact analysis for nucleic acids and their complexes. *Nucleic Acids Res.* **32**, W615–W619 (2004).
60. DeLano, W.L. *The PyMOL Molecular Graphics System* (DeLano Scientific, San Carlos, CA, 2002).